International Journal of Modern Physics E
Vol. 24, No. 11 (2015) 1550084 (15 pages)

DOI: 10.1142/S0218301315500846

Target productions in forward and backward hemispheres in the interactions of ^{28}Si-EM at 14.6A GeV

A. Abdelsalam
Physics Department, Faculty of Science, Cairo University, Giza, Egypt
Abdallaham@hotmail.com

M. S. El-Nagdy
Physics Department, Faculty of Science, Helwan University, Helwan, Egypt
Physicshelwan@yahoo.com

A. M. Abdalla* and A. Saber†
Mathematics and Physics Engineering Department,
Faculty of Engineering in Shoubra, Banha University, Cairo, Egypt
**a_abdalla65@hotmail.com*
†*nasser.s2009@yahoo.com*

Received 14 September 2014
Revised 20 September 2015
Accepted 22 September 2015
Published 9 November 2015

This paper search for the results and properties of slow particle productions, appear as a gray and black tracks in nuclear emulsions, producing secondary charged particles which are emitted from ^{28}Si interactions with emulsion nuclei at 14.6A GeV. The forward particles emission of interactions, ($\theta_{\text{lab}} < 90^\circ$) as well as the backward ones ($\theta_{\text{lab}} \geq 90^\circ$), have been investigated. It includes the effect of both projectile mass number and energy on the production and multiplicities of these particles. The results compared with other experiments for the same target but with different projectiles and energies. The experimental data show that there are two different mechanisms responsible for the production of gray particles for the chosen channels of emission angles and each are energy dependence. This dependence is weakly on the projectile mass number. The same investigations are applied for black tracks producing particles. The experimental results show the production of these particles is purely target fragments independent on both projectile mass number and its energy. The anisotropy ratio of angular distribution (F/B) is applied for both kinds of particles which are found the value for gray particle production depends on the direction of emissions while it is unchanged for black particles.

Keywords: Slow fragments; particles multiplicities; forward and backward emission angles.

PACS Number: 25.75.−q

*Corresponding author.

1. Introduction

One of the particular interests at high-energy nucleus–nucleus collisions results from the expectations of the collective phenomena. It allows strong interactions in which nuclear matter undergoes a phase transition to quark–gluon plasma at very high temperature $\sim 200\,\text{MeV}$ or energy densities $\sim(2\text{–}3)\epsilon_\circ$.[1] The characteristic feature of this matter beyond the productions of excited baryonic and mesonic states is the individual nucleon–nucleon collisions. As a result, nucleons and hadrons are observed over a wide range of energies and angles.[2] This paper presents the experimental properties of slow fragments ($E \leq 400\,\text{MeV}$) which are produced from ^{28}Si collisions with composite target emulsion nuclei at energy $14.6A$ GeV per nucleon. The multiplicities of secondary slow particles are classified according to their emission angles θ, which are measured from direction of incident projectile. First, is forward hemisphere (FHS), those are particles with $\theta_{\text{lab}} < 90^\circ$ and second backward hemisphere (BHS) with $\theta_{\text{lab}} \geq 90^\circ$. It is important to study experimental features and search for the physical system responsible for production of these fragments. Experimentally, it is possible to distinguish between projectile and target fragments where the projectile spectator fragments are mainly those emitted in a narrow cone where $\theta_{\text{lab}} \leq 13$ mrad at energy $14.6A$ GeV[3–5] while target fragments essentially emitted in a wide range of angles as evaporated fragments from the residual nucleus and rescattering or knock out protons and slow mesons. The dependences of the production of these particles and their multiplicities on the projectile mass numbers and energies are also investigated.

2. Theoretical Considerations

Many theoretical models succeeded to describe the multiplicities of different secondary particle productions.[6–15] These models are used to describe the high-energy components of newly created hadrons and many particles resulting from the nuclear disintegration following the high-energy collisions. Models for nuclear evaporation and fragmentation and for high-energy fusion are however usually included in hadrons cascade model.[16,17] This is not appreciable in the multi GeV energy range of present experiment. The intra-nuclear cascade models have been greatly improved[18–21] and their range of validity can be extended to higher energies due to the introduction of the formation zone concept.[22–24] The cascade protons have energies, which are typical for the so-called gray prongs, observed in emulsion experiments. Therefore, it is possible to calculate the nuclear excitation energy of the residual nucleus then the nuclear evaporation and high-energy fission reaction.

In any particular Lorentz frame, it is possible to follow the trajectories of the secondaries created in the hadronization of the chains in space and time. By considering the relativistic time dilation, secondaries with high energies in the nucleus rest systems mostly formed outside the nucleus therefore they are not able to initiate intra-nuclear cascade processes. On the other hand, the lower energy of the secondary hadronic system has higher probability to form hadrons inside the nucleus.

These hadrons may re-interact with spectator nucleons taking into account nuclear geometry. All these properties of secondary particles production are explained in terms of analysis of the experimental results, which will be discussed in Sec. 5 in this paper.

3. Production of Proton in the Backward Hemisphere

The phenomenon of backward particle emission in heavy ion reactions has attracted much attention from both the theoretical and experimental point of view.[2] Several publications are introduced for the last four decades concerning the experiments, done at Berkeley and JINR and studied the production mechanism of hadrons in the BHS. Throughout, those studies of the backward particle emission (i.e. the particles emitted beyond the kinematics limit of those are expected to emit from simple nucleon–nucleon collisions).

The backward proton emission is strictly forbidden for free nucleon–nucleon collision, therefore, the production of such protons from nucleus–nucleus collisions may reflect nuclear effects such as the internal motion of nucleons inside the nucleus and short-range correlation between nucleons or multiple nucleon–nucleon collision effects.[6] Therefore, study of the characteristics of the energetic protons emitted in the backward direction through the heavy ion collisions supplies effective information on nuclear effects. In the incident energy limit ($E < 1$ GeV per nucleon); Frankel has interpreted the data in terms of the quasi-two-body-scaling model,[7] in which the primary mechanism for backward proton productions is a scattering between the incident nucleons and the target nucleons. They are target nucleons, which boosted onto the mass shell and appeared in the backward direction. Frankel was able to reproduce the low energy data by a simple structure function and suggested that this function was a measure of the internal momentum distribution of nucleons inside the target.

Several experiments have been done at Berkeley and JINR[8] for systematic study of the backward protons. The obtained data show that, the characteristic spectrum of the emitted protons with momentum above 400 MeV/c is independent of the projectile type and incident energy. All experimental data[9] on the backward proton characteristic above 2 GeV/nucleon give an evidence for the limiting fragmentation hypothesis,[10] which implies that, both projectile and target may fragment irrespective of each other. Fujita and Hüfner[25] suggested a model for backward proton emission mechanism, which includes both initial correlations between nucleons in the target and final correlations between two nucleons. The final state of interaction with the rest of the target nucleons (A-2) is neglected where A is the target mass number. Fujita[26] has extended this model to include multiple correlations. The improved model described well the data for the backward proton production at the incident energy less than 1 GeV. A theoretical work by Frankfurt and Strikman[27] beside Yukawa and Furui[28] indicated that, the backward proton spectra induced by high-energy probes are mainly composed of spectator nucleons from

the breakup of correlated pairs in the nucleus. As such, these backward nucleons potentially reflect direct information of the nuclear wave function. Schroeder *et al.*,[8] presented an experiment held at Berkeley[29] in order to obtain more information on the mechanisms responsible for high energy backward particle production by bombarding 2.1 GeV proton with various targets. At first, they found large fraction of the events ($\approx 50\,\%$), to have an associated negative track, which could be identified as a pion. Typically, that pion appeared at $\theta_{\rm lab} < 90^\circ$. Thus, backward particles emission (typically the backward track is a proton) at 2.1 GeV is often accompanied by the production of a pion. They suggested that the simple quasi-elastic process, $NN \rightarrow NN$, as suggested by Frankel,[7] was not the dominant mechanism at that energy for producing backward protons. On this way, the authors in Ref. 30, studied the results obtained from the experiments using nuclear emulsion, concluded that, the dependence of the backward emission of different particles on the projectile is weaker than that in the forward emission and also the backward emission tends to depend on the target size. In the same time they concluded that, the characteristics of particles emitted in the BHS are completely different from those emitted in the FHS. Therefore, the BHS is intimately connected with the target fragmentation region i.e. with that part of the phase space where all single particle characteristics are most safe from being dependent on the projectile in accordance with the limiting fragmentation hypothesis when applying to nuclei.[2]

4. Experimental Details

In the present work, stacks of FUJI type of nuclear emulsion was exposed to the 14.6A GeV ^{28}Si beam at Brookhaven National Laboratory (BNL) Alternating Gradient Synchrotron (AGS). Each emulsion pellicle of the stack has 600 μm thickness and $20 \times 10\,{\rm cm}^2$ dimensions. The emulsion pellicles was doubly scanned along the tracks, fast in the forward direction and slowly in the backward one. The scanning of the emulsion pellicles was carried out using a 850056 STEINDORFF microscope. It has a stage of $18 \times 16\,{\rm cm}^2$ with an opening of $7 \times 2.5\,{\rm cm}^2$, stage adjustment in the x-direction is possible over a total length of 7.8 cm with a reading accuracy of the order 0.1 mm. The total scanned length 121.8 m and 962 inelastic interaction were detected. The experimental technique, method of measurements and primary results of the experiment are explained in details in Refs. 31–33.

When charged particle passes through the photographic nuclear emulsion, it will slow down via losing its kinetic energy due to its inelastic interactions with the nuclear emulsion atoms along its path. The charged particle loses its kinetic energy via the ionizations of the grains of silver halides and via multiple elastic and inelastic scattering, which leads to trails of ionized silver halides along its path. The grain density is defined as the number of developed grains of silver halides per unit path length of the particle's track. It is denoted by (g) in a track corresponding to a particular value of specific ionization of such particle, so obviously it depends on some factors such as the degree of the development of the nuclear emulsion, the

velocity and the charge of the ionizing particle. In order to obtain high accurate results, determine the normalized grain density g^* where, $g^* = g/g_o$. The value g, is the observed grain density per 100 μm for the emitted secondary particles after performing the dip angle correction. The magnitude, g_o is the grain density per 100 μm of the energy relativistic track of minimum ionization i.e. singly charged particle or electron. Both values of g and g_o are counted in the same plateau region and at the same depth in the nuclear emulsion. The tracks of the secondary charged particles, which are produced, are classified into three types according to the normalized grain density g^*. The secondary charged particles are classified according the grain densities into the categories as follows:

(1) The Shower Tracks are characterized by the value of the normalized grain density ($g^* \leq 1.4$) and very high value of the velocity ($\beta = v/c \geq 0.7$). Most of the shower particles are mesons with energy ($E > 50$ MeV) contaminated with small fraction of fast protons with energy ($E > 400$ MeV), charged K-mesons, antiprotons and hyperons. The shower particles multiplicities are denoted by (n_s), which its value gives good estimates of the number of the charged π-mesons produced in the interaction.
(2) The gray tracks are characterized by the value of the normalized grain density ($1.4 < g^* \leq 10$), the value of the velocity ($0.3 < \beta < 0.7$), where most of them are recoil protons having range in the nuclear emulsion ($L > 3000\,\mu$m), which corresponds to proton energies in the range from 26 MeV up to 400 MeV. Some of the gray tracks may be due to emitted deuterons, tritons, helium nuclei and nearly about (5%) due to slow π-mesons. The gray tracks multiplicity is denoted by (N_g).
(3) The black tracks are characterized by the value of the normalized grain density ($g^* \geq 10$), the value of the velocity ($\beta \leq 0.3$), where most of them are due to protons having "Range" in the nuclear emulsion ($L \leq 3000$), which corresponds to proton energies ($E < 26$ MeV). The black tracks may be also due to deuterons, α-particles and heavy fragments. (N_b) denotes the black tracks multiplicity. The gray tracks and the black tracks are known as tracks of the heavily ionizing particles with the value of the velocity ($\beta < 0.7$). The heavily ionizing particles multiplicity is denoted by (N_h), where $N_h = N_g + N_b$.

5. Experimental Results and Discussions

5.1. *Gray particle multiplicity*

First, we will concern with gray particle productions emitted in all angles of emission from two silicon beams, at different energies 14.6 GeV per nucleon (this work) and 3.7 GeV from Ref. 34. The multiplicity distributions of gray particles are shown in Fig. 1. The average multiplicities are given in Table 1. It clears that, on the average, the multiplicities of gray particles are weakly energy dependent. The two distributions can fit as exponential curve, which reflects that the mechanism responsible for

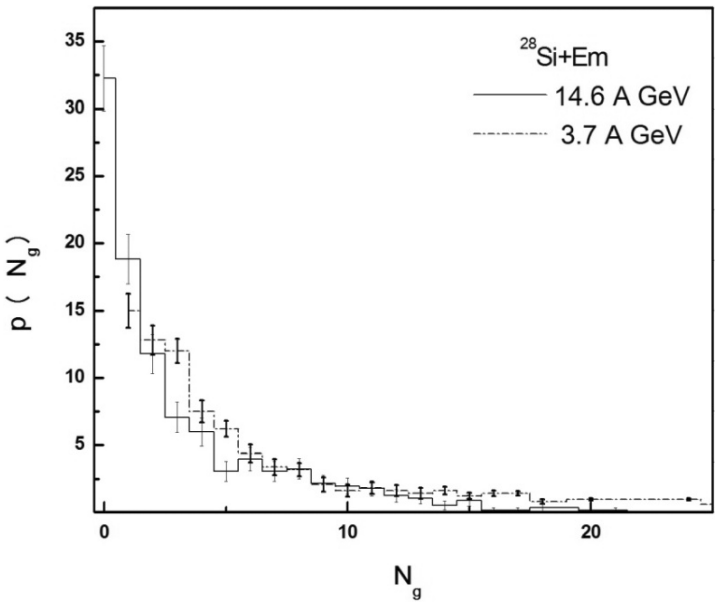

Fig. 1. The normalized multiplicity distributions for the gray particles through the interactions of ^{28}Si with emulsion nuclei at 14.6A GeV in comparison with the corresponding data for ^{28}Si-Em at 3.7A GeV.

Table 1. Average multiplicity of gray particles emitted from Si-Em interactions at 3.7 and 14.6A GeV.

Energy GeV/A	$\langle N_g \rangle$	Ref.
3.7A GeV	6.90 ± 0.20	34
14.6A GeV	3.01 ± 0.16	This work
	5.40 ± 0.20	34
	2.97 ± 0.14	35

production of gray particles is regular and takes uniform decay rates. This means that the mechanism of intra-nuclear cascade for projectile nucleons inside target nucleus plays the main reason for gray particle production as slow particles and knocks out protons emitted from target fragments. This production is regular and the frequencies of its production are uniformly decreased with high multiplicity and weakly dependent on projectile energy.

Now, multiplicities of gray particles at two silicon energies are classified into two categories, one that is produced in FHS, are shown in Fig. 2(a) and the BHS are shown in Fig. 2(b). The corresponding mean values are given in Table 2. The data for gray and black particle emission in FHS and BHS at energy 3.7A GeV is collected from Ref. 39. It is noticed that for both two ^{28}Si beams, the forward gray particle multiplicity is weakly energy dependent while this is not observed for production of the backward particles. This behavior may be explained in terms of

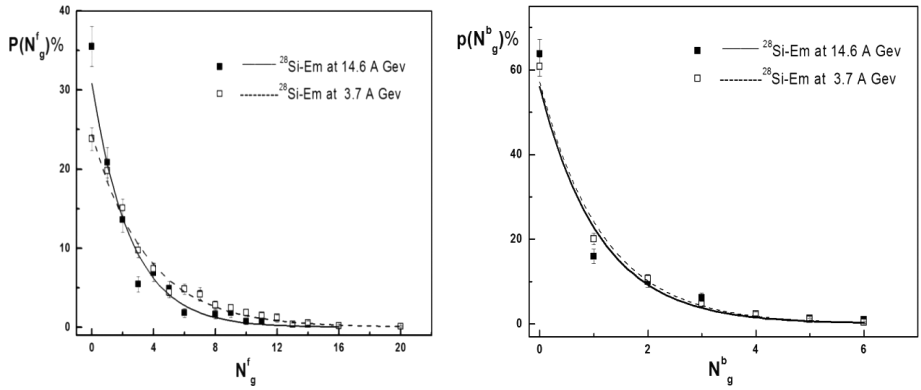

(a) (b)

Fig. 2. The normalized multiplicity distributions of the gray particles emitted (a) in FHS (b) in BHS through the interactions of ^{28}Si at (3.7 and 14.6A GeV) with emulsion nuclei together with the smooth fitting curve.

increasing projectile energy, which allow participant of both projectile and target nucleons to have enough energy to make a series of secondary collisions. These collisions are responsible for creation of new hadrons and producing a large number of fast protons, observed experimentally in forward direction. The mechanism of interactions is merely different in the backward BHS. The two projectile energies are sufficient to reach states at which participant nuclear matter becomes at a relative high-energy states and nonthermal equilibrium. These states are responsible for producing target fragments. It explains the possibility of limiting fragmentation for target nucleus.

The previous exponential rate for losing energy may take a form of production of gray particles emitted in directions independent on the direction of the incident projectile. The loss of energy for forward and backward directions can be represented in terms of the multiplicities in both directions and using the normal distribution of energy as a decay curve takes the form:

$$P(N_g^i) = \alpha_g^i e^{-\lambda_g^i N_g^i}, \tag{1}$$

where, α_g^i and λ_g^i are the fitting parameters. [g (gray)] and [$i = f$ (forward), b(backward)]. The value of α_g^i and λ_g^i for both silicon beams are given in Table 2.

Within experimental errors, the values λ_g^i, in the forward direction are less than that in the backward and both values are weakly increased with projectile energy. This is because the energy transfer to the participant target nucleons is sufficient to make many fast recoil protons in the forward where the longitudinal momentum reaches to maximum in the direction of the projectile while in the backward direction, the interactions do not have enough energy to make successive collisions and hence the number of knock out protons decreases. The values of parameter α_g^i for backward direction are higher than that for the forward ones for

Table 2. The average multiplicities and fitting parameters of forward and backward emitted gray particle distributions fitted by an exponential decay law form.

Projectile	Energy GeV/A	$\langle N_g^f \rangle$	$\langle N_g^b \rangle$	α_g^f	λ_g^f	α_g^b	λ_g^b	Ref.
^{12}C	3.7	4.52 ± 0.20	1.38 ± 0.07			45.92 ± 11.56	0.75 ± 0.06	36–39
^{16}O	3.7	4.47 ± 0.13	1.22 ± 0.04			44.76 ± 1.33	0.60 ± 0.02	36–40
^{22}Ne	3.3	4.80 ± 0.20	1.42 ± 0.08			40.91 ± 7.58	0.66 ± 0.04	36–38, 41
^{28}Si	3.7	4.98 ± 0.18	1.42 ± 0.07	24.35 ± 0.62	0.28 ± 0.01	42.11 ± 8.88	0.67 ± 0.04	36–39
^{28}Si	14.6	2.26 ± 0.13	0.74 ± 0.05	30.85 ± 1.88	0.41 ± 0.13	55.97 ± 3.08	0.90 ± 0.04	This work

Table 3. The average multiplicity of the gray particles emitted in FHS and BHS from different projectiles interactions with emulsion nuclei at high energy.

Projectile	Energy GeV/A	$\langle N_g^f \rangle$	$\langle N_g^b \rangle$	$\langle N_{\rm int} \rangle$	$(\mathrm{F/B})_g$	χ_o^g	$\beta_{//}^g$	Ref.
^{6}Li	3.7	2.08 ± 0.08	0.98 ± 0.05	3.56	2.12 ± 0.13	0.33	0.11	42, 43
^{12}C	3.7	4.52 ± 0.20	1.38 ± 0.07	5.88	3.27 ± 0.19	0.52	0.18	36–41
^{22}Ne	3.3	4.80 ± 0.20	1.42 ± 0.08	8.98	3.38 ± 0.28	0.54	0.19	36–38, 41
^{28}Si	3.7	4.98 ± 0.18	1.42 ± 0.07	10.43	3.52 ± 0.28	0.55	0.19	36–38, 41
^{28}Si	14.6	2.26 ± 0.13	0.74 ± 0.05	10.43	3.05 ± 0.27	0.49	0.17	This work
^{32}S	3.7	3.17 ± 0.14	0.82 ± 0.05	14.68	3.86 ± 0.29	0.52	0.18	39, 41

the two values of projectile energies. Other point of view is the weak dependence of α_g^b and λ_g^b on the projectile mass number for both directions. This behavior may be explained by considering that the increasing of the number of participant nucleons, leads to increase of secondary interactions, which are the responsible parameter for gray particles emission in a wide range of angles which are independent on the direction of incident projectile.

Table 3 gives the average values of the gray particle multiplicities, emitted in FHS and BHS, for the interactions of the present $14.6A$ GeV ^{28}Si in nuclear emulsion compared with the corresponding due to the interactions of different projectiles with emulsion nuclei at energy 3.3 to $14.6A$ GeV. There is a weekly change for both directions on projectile mass number.

Other point of view is studying the probability of the emission mechanism responsible for gray particle production using statistical model.[44] This model depends on Maxwell distribution for momentum P of the emitted fragments. This distribution can be expressed in terms of the dimensionless fragment velocity β and take the form

$$\frac{dN^2}{d\beta\, d\mu}\alpha \exp\left[-\left(\beta^2 - 2\beta_{\|}\beta_{\mu}\right)/\beta_0^2\right],$$

where $\beta_{\|}$ is normally the longitudinal velocity of the particle emitting system. $\mu = \cos\theta$ where θ is the laboratory angle between the momentum of the fragment of mass M and momentum of the initial projectile and $P_0 = M\beta_0 = \sqrt{2ME_0}$ where E_0 is the characteristic energy per particle in this hypothetical moving system. The parameters $\beta_{\|}$ and β_0 take the values characterizing the angular distribution of the fragments. The forward to backward ratios $(\mathrm{F/B})_g$, which are defined as the ratios between the average multiplicities of the forward emitted gray particles to those of backward ones, are displayed in Table 3. The $(\mathrm{F/B})_g$ represents the anisotropy ratio of angular distribution, which are determined according to statistical model by the following equations,

$$(F/B)_g \approx \exp\left(\frac{4}{\sqrt{\pi}}\chi_0^g\right), \tag{2}$$

where, χ_o^g is the predicted rational velocity.

$$\chi_o^g = \beta_{//}^g/\beta_o^g, \tag{3}$$

where, $\beta^g_{//}$ is the mean longitudinal velocity of the center mass of the gray particle emission system and β^g_o is the characteristic spectral velocity of the fragmentation system of gray particles. The used value of β^g_o is ≈ 0.35, as given in Ref. 45. The values of $\beta^g_{//}$ can be calculate from Eq. (3). From Table 3 one can notice that,

- The dependence of $\langle N^f_g \rangle$ on projectile mass number is observed than that for $\langle N^b_g \rangle$ and hence the same notice on the mean value of geometrical interacting nucleon $\langle N_{\rm int} \rangle$
- The values of $\langle N^f_g \rangle$ are nearly three times greater than $\langle N^b_g \rangle$ for all projectiles.
- The result is reflected on the $(\mathrm{F/B})_g$ ratio and consequently on the values of χ^g_0 which tend to be nearly constant for all projectiles. Therefore, mainly one concludes that, the dependence of the fast target fragments (g-particles) in FHS and BHS on the projectile sizes is nearly weak.
- The values of χ^g_o are approximately equal to 0.5 for all given projectiles.
- The emitting system of the gray particles is fast with typical longitudinal velocities $\beta^g_{//} \approx 0.13$–$0.22$

It is important to study the properties of the gray particle emission in terms of impact parameter of nucleus–nucleus collisions. In emulsion experiments, the multiplicity of heavily ionizing charged particles N_h is considered as target fragment and it's used as indication to describe the degree of overlapping for projectile and target nuclei. Figure 3 shows the correlation of mean values of gray particle produced in forward and in BHS with N_h multiplicity. This dependence can be represented by a linear fitting in a form as $\langle N^i_g \rangle = A + BN_h$ where i take forward f and backward b. Table 4 gives the magnitudes of A and B, for both directions. The magnitude of

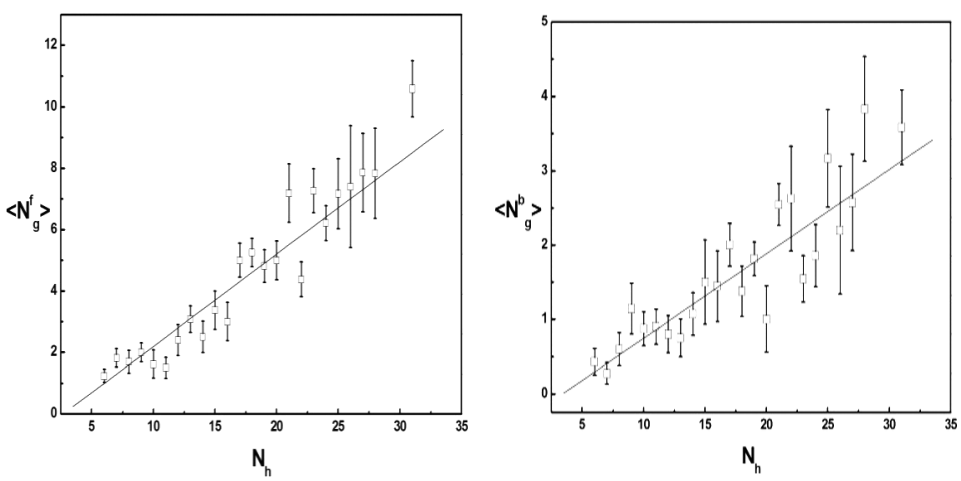

(a) (b)

Fig. 3. The correlation of mean gray tracks multiplicity for FHS and BHS on multiplicity of heavily ionizing charged particles.

Table 4. Slop B and intercept A of the fitting parameter for both forward and backward gray particle productions.

	A	B
$\langle N_g^f \rangle$	-0.81 ± 0.3	0.3 ± 0.02
$\langle N_g^b \rangle$	-0.39 ± 0.15	0.11 ± 0.01

parameter B means the rate of gray particle production with impact parameter in forward takes 3 times as the corresponding value in backward.

5.2. *Black particle multiplicity*

Second, in this section we will study the properties of the collisions responsible for production of slow particles, which appear as black tracks in emulsion experiments. These particles play an important role to describe the mechanism of the interactions between projectile and target nuclei. It is mainly target fragments emitted during the last stage of interactions as an evaporated particle from residual target nucleus. It contains massive particles with minimum energy emitted in a wide range of angles, which are independent on direction of the incident projectile especially more heavy black fragments. The multiplicity distributions for black particle productions in both two-silicon energies are shown in Fig. 4. The average values of the multiplicity are given in Table 5. There is no clear dependence on projectile energy and the average multiplicities are nearly constant. This proves that the multiplicity of these particles is energy independent and purely depends on the of target nucleus. Its multiplicity is explained in terms of the limiting values of target-evaporated fragmentations. The black particle productions in both FHS and BHS directions emitted from two silicon beams are shown in Fig. 5

The dependence on multiplicity distributions for black particle production in the forward on the projectile energy is weak while it is completely absent in the backward direction. The exponential decay represented by Eq. (1) can be applied for black particle multiplicity where the fitting parameters α_b^i and λ_b^i are given in Table 6. This table contains the corresponding parameters for different projectiles (^{3}He, ^{4}He, ^{6}Li, ^{7}Li and ^{32}S) at nearly the same energy. From Table 6, the magnitudes of parameters α_b^f and λ_b^f are nearly constant for all projectiles independent on projectile mass number but they slightly increase in backward than that in the forward. It may be explained by considering that the black fragments are produced from hot residual target nucleus during evaporation and cooling mechanisms. Hence, the mechanism responsible for producing black particles in FHS may be similar to that in BHS.

The predicted rational velocity, χ_o according to statistical model calculated from Eqs. (2) and (3) is applied for black particles where it represents the ratio of the longitudinal velocity of the center-of-mass $\beta_{//}^b$, to the characteristic spectral

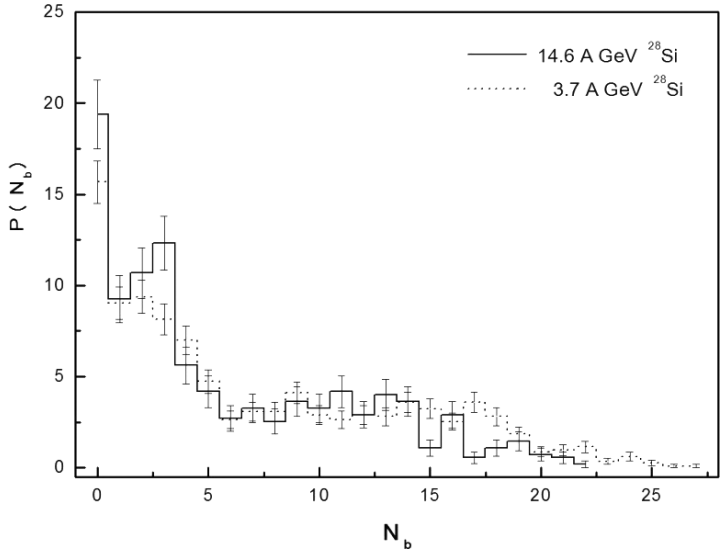

Fig. 4. The normalized multiplicity distributions of the black particles through the interactions of ^{28}Si at (3.7 and 14.6A GeV) with emulsion nuclei.

Table 5. The average values of multiplicities of the black particles from ^{28}Si-Em interactions at 14.6 and 3.7A GeV and also the corresponding values for FHS and BHS.

Energy GeV/A	$\langle N_b \rangle$	$\langle N_b^f \rangle$	$\langle N_b^b \rangle$	Ref.
3.7A GeV	7.14 ± 0.20	4.39 ± 0.13	2.76 ± 0.08	36–38
14.6A GeV	5.67 ± 0.24	3.17 ± 0.14	2.51 ± 0.12	This work

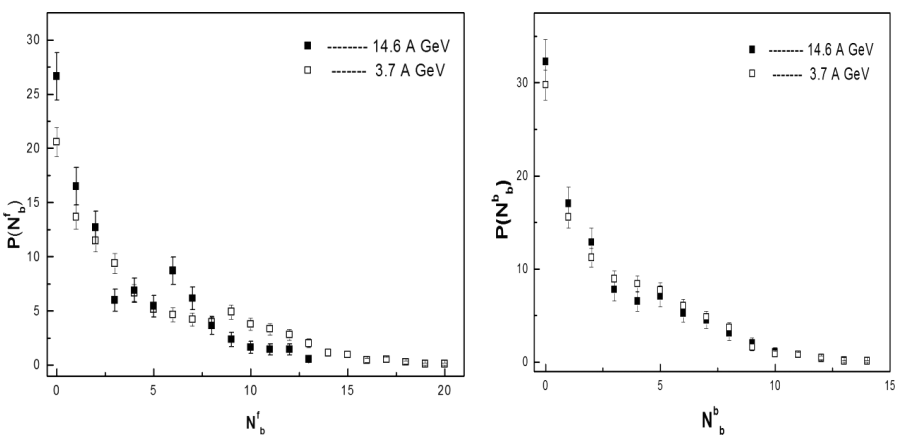

(a) (b)

Fig. 5. The normalized multiplicity distributions of the black particles emitted (a) in FHS (b) in BHS through the interactions of ^{28}Si at (3.7 and 14.6A GeV) with emulsion nuclei together with the smooth fitting Curve.

Table 6. The characteristic parameters of multiplicity distributions of black particles emitted in FHS and BHS through nucleus–nucleus interactions at high energy.

Projectile	Energy (GeV/A)	α_b^f	λ_b^f	α_b^b	λ_b^b	Ref.
^{3}He	3.7	21.90 ± 0.74	0.25 ± 0.01	28.17 ± 0.94	0.34 ± 0.01	46
^{4}He	3.7	25.63 ± 1.08	0.31 ± 0.01	30.78 ± 1.26	0.38 ± 0.01	46
^{6}Li	3.7	25.69 ± 1.09	0.30 ± 0.01	31.82 ± 1.31	0.40 ± 0.01	41
^{7}Li	2.2	22.38 ± 0.98	0.26 ± 0.01	29.80 ± 1.27	0.36 ± 0.01	41
^{28}Si	3.7	18.24 ± 4.72	0.21 ± 0.01	26.07 ± 1.04	0.33 ± 0.01	36–38
^{28}Si	14.6	21.23 ± 1.35	0.25 ± 0.24	26.78 ± 1.59	0.32 ± 0.16	This work
^{32}S	3.7	16.25 ± 0.96	0.20 ± 0.01	25.34 ± 1.37	0.32 ± 0.01	41–43

Table 7. The average multiplicity of the black particles emitted in FHS and BHS from the interactions of different projectiles with emulsion nuclei at high energy.

Projectile	Energy (GeV/A)	$\langle N_b^f \rangle$	$\langle N_b^b \rangle$	$(\mathrm{F/B})_{\mathrm{b}}$	χ_o^b	$\beta_{//}^{\mathrm{b}}$	Ref.
^{3}He	3.7	3.46 ± 0.09	2.39 ± 0.06	1.46 ± 0.05	0.17	0.018	46
^{4}He	3.7	2.90 ± 0.10	2.18 ± 0.08	1.33 ± 0.07	0.13	0.014	46
^{6}Li	3.7	2.84 ± 0.09	2.18 ± 0.07	1.29 ± 0.06	0.12	0.013	40
^{7}Li	2.2	3.39 ± 0.12	2.29 ± 0.08	1.48 ± 0.07	0.17	0.018	40
^{28}Si	3.7	4.39 ± 0.13	2.76 ± 0.08	1.59 ± 0.07	0.17	0.018	36–38
^{28}Si	14.6	3.17 ± 0.14	2.51 ± 0.12	1.26 ± 0.08	0.11	0.012	This work
^{32}S	3.7	4.63 ± 0.18	2.93 ± 0.12	1.58 ± 0.09	0.21	0.023	41, 42

velocity, β_o^b of the fragmentation system of black particles. The value of $\beta_o^b \approx 0.11$ used from Ref. 45. The ratios of the average multiplicities in both directions, F/B, are given in Table 7. The magnitudes of $(\mathrm{F/B})_b$, χ_o^b and β_o^b for different projectiles are nearly constant which proves that there is a constant mechanism responsible for of black particle evaporation and it's independent on projectile mass number. The longitudinal velocity parameter is the same for this range of energy and projectile mass number. It can be explained in terms of the homogenous distribution for the emission of target fragments and independently on the angles of emission.

6. Conclusion

Many experimental observations can be concluded as the following:

- There are two different mechanisms responsible for gray particle productions in forward and backward directions. Both mechanisms can be represented by exponential decay functions with fitting parameters depended on the direction of the emission of the particles.
- The anisotropy ratio of angular distribution $(\mathrm{F/B})_g$, determined according to statistical model which describes the ratio of the mean longitudinal velocity of the center-of-mass for gray particle emission system to the characteristic spectral velocity of the fragmentation system is nearly constant in the energy range 3.7–14.6A GeV

- The mechanism in forward direction is more dependent on projectile energy than in the backward one.
- The emission of the black particles is independent on the projectile energy and mass number. It concludes that, the production of these particles is purely target fragments and there is a limiting value of target fragmentations.
- The ratio $(F/B)_b$ for black particle production is nearly constant and independent on the angle of emission. It proves that, the mechanism responsible for production of these particles is independent on the direction of the incident projectile.

Acknowledgment

The authors would to thank P. L. Jain for their supplements of the irradiated emulsion plates.

References

1. S. K. Karn, R. S. Kaashal and Y. K. Mathur, *Z Phys. C* **72** (1996) 297, doi:10.1007/s002880050249.
2. A. Abdelsalam, M. Šumbera and S. Vokál, JINR, El 82–509, Dubna (1982).
3. M. I. Adamovich *et al.*, *Z. Phys. A* **351** (1995) 311.
4. M. I. Adamovich *et al.*, *Phys. Lett. B* **223** (1989) 262.
5. M. I. Adamovich *et al.*, JINR, E1 92–569, Dubna (1992).
6. S. Nagamia *et al.*, *Phys. Rev. C* **24** (1981) 971.
7. S. Frankel, *Phys. Rev. Lett.* **38** (1977) 1338.
8. L. S. Schroeder, Berkeley Preprint–LBL 11102, Nuclear Studies, Kikuchi Summer School on Nuclear Physics at High Energies, Fuji–Yoshida, Japan, July 1–4 (1980).
9. Yu. D. Bayukov *et al.*, *Phys. Rev. C* **20** (1979) 764.
10. M. L. Perl, *High Energy Hadron Physics* (John Wiley and Sons, New York, 1974), p. 201.
11. A. Capella, U. Sukhatme, C. I. Tan and J. Tran Thanh Van, *Phys. Rep.* **236** (1994) 227.
12. P. Aurenche, F. W. Bopp, A. Capella and J. Tran Thanh Van, *Phys. Rev. D* **45** (1992) 92.
13. F. W. Bopp, R. Engle, D. Pertermann and J. Ranft, *Phys. Rev. D* **49** (1994) 3236.
14. H. J. Möhring and J. Ranft, *Z. Phys. C* **52** (1991) 643.
15. J. Ranft, *Phys. Rev. D* **51** (1995) 64.
16. H. W. Bertini, *Phys. Rev.* **137** (1963) 1801.
17. H. W. Bertini, *Phys. Rev.* **188** (1969) 1711.
18. A. Fassò, A. Ferrari, J. Ranft and P. R. Sala, FLUKA: Present status and future developments, in *Proc. 4th Int. Conf. Calorimetry in High Energy Physics*, La Biodola (Elba), Italy, 1993, eds. A. Menzione and A. Scribano (World Scientific, 1994), p. 493.
19. A. Fassò, A. Ferrari, J. Ranft and P. R. Sala, FLUKA: Performances and Applications in the Intermediate Energy Range, in *Proc. Specialists Meeting on Shielding Aspects of Accelerators, Targets & Irradiation Facilities* (Arlington, USA, 1994), published by OECD/NEA (1994), p. 287.
20. P. A. Aarnio *et al.*, in *Proc. Int. Conf. Monte Carlo Simulation in High Energy and Nuclear Physics*, MC'93 (Tallahassee, USA, 1993), eds. P. Dragovitsch, S. L. Linn and M. Burbank (World Scientific, 1994), p. 88.
21. Y. Yariv and Z. Fraenkel, *Phys. Rev. C* **24** (1981) 488.

22. L. Stodolski, *Proc. 5th Int. Colloquium on Multi-Particle Reactions* (Oxford, 1975), p. 577.
23. J. Ranft, *Z. Phys. C* **43** (1989) 439.
24. J. Ranft, *Phys. Rev. D* **37** (1988) 1842.
25. T. Fujita and J. Hüfner, *Nucl. Phys. A* **314** (1979) 317.
26. T. Fujita, *Nucl. Phys. A* **324** (1979) 409.
27. L. L. Frankfurt and M. I. Strikman, *Phys. Lett. B* **83** (1979) 497.
28. T. Yukawa and S. Furui, *Phys. Rev. C* **20** (1979) 2316.
29. L. S. Schroeder, *Nucl. Ins. Methods* **162** (1979) 385.
30. N. Ali-Moussa, *Arab. J. Nucl. Sci. Appl.* **33**(1) (2000) 211.
31. M. El-Nadi, M. S. El-Nagdy, N. Ali-Mossa, A. Abdelsalam, A. M. Abdalla and A. A. Hamed, *J. Phys. G*, *Nucl. Phys.* **25** (1999) 1169.
32. M. El-Nadi *et al.*, *Eur. Phys. J. A-Hadrons and Nuclei* **10**(2) (2001) 177.
33. M. El-Nadi *et al.*, *J. Phys. G*, *Nucl. Part. Phys.* **28**(6) (2002) 1251.
34. M. I. Adamovich *et al.*, Communication of the Joint Institute for Nuclear Research Dubna E1-92 (1992) 569.
35. M. S. EL-Nagdy, A. Abdelsalam, N. Ali-Mossa, A. M. Abdalla, S. M. Abdal-Halim and K. Abdel-Waged, *Nucl. Phys. A* **370** (2004) 419.
36. M. El-Nadi, A. Abdelsalam and N. Ali-Moussa, *Int. J. Mod. Phys. E.* **3** (1994) 811.
37. M. El-Nadi, A. Abdelsalam and N. Ali-Moussa, *Radiat. Phys. Chem.* **47** (1996) 681.
38. M. El-Nadi, A. Abdelsalam and N. Ali-Moussa, *IL Nuovo Cimento A* **110** (1998) 1255.
39. A. Abdelsalam, E. A. Shaat, N. Ali Mossa, Z. Abou-Moussa, O. M. Osman, N. Rashed, W. Osman, B. M. Badawy and E. El-Falaky, *J. Phys. G* **28** (2002) 1375.
40. LI. Hui-Ling, Z. Dong-Hai and LI. Jun-Sheng, *Chin. J. Phys. C* (HEP&NP) **33** (2009) 521.
41. A. Abdelsalam, B. M. Badawy and E. El-Falaky, *Can. J. Phys.* **85** (2007) 837.
42. M. El-Nadi, A. Abdelsalam, N. Ali-Moussa, Z. Abou-Moussa, S. Kamel, K. Abdel-Waged, W. Osman and Badawy, *Eur. Phys. J. A* **3** (1998) 183.
43. M. El-Nadi, A. Abdelsalam, N. Ali-Moussa, Z. Abou-Moussa, S. Kamel, Kh. Abdel-Waged, W. Osman and B. M. Badawy, *IL Nuovo Cimento A* **111** (1998) 1243.
44. H. H. Hackmann, H. J. Crawford, D. E. Greiner, P. J. Lindstrom and W. Wilson Lamce, *Phys. Rev. C* **17** (1978) 1651.
45. A. Abdelsalam, *Phys. Scr.* **47** (1993) 505.
46. A. Abdelsalam, M. S. El-Nagdy, N. Rashed, B. M. Badawy and E. El-Falaky, *J. Nucl. Radiat. Phys.* **2** (2007) 49.